Inorganic Chemistry

ARTICLE

pubs.acs.org/IC

Stabilization and Study of $SrFe_{1-x}Mn_xO_2$ Oxides with Infinite-Layer Structure

María Retuerto,[*,†,§] Félix Jiménez-Villacorta,[‡] María J. Martínez-Lope,[§] María T. Fernández-Díaz,[⊥] and José A. Alonso[§]

[†]Department of Chemistry and Chemical Biology, Rutgers, the State University of New Jersey, 610 Taylor Road Piscataway, New Jersey 08854-808, United States

[‡]Department of Chemical Engineering, Northeastern University, Boston, Massachusetts 02115, United States

[§]Instituto de Ciencia de Materiales de Madrid, CSIC, Cantoblanco, E-28049 Madrid, Spain

[⊥]Institut Laue-Langevin (ILL), BP156X, Grenoble F-38042, France

ABSTRACT: A series of layered oxides of nominal composition $SrFe_{1-x}Mn_xO_2$ (x = 0, 0.1, 0.2, 0.3) have been prepared by the reduction of three-dimensional perovskites $SrFe_{1-x}Mn_xO_{3-\delta}$ with CaH_2 under mild temperature conditions of 583 K for 2 days. The samples with x = 0, 0.1, and 0.2 exhibit an infinite-layer crystal structure where all of the apical O atoms have been selectively removed upon reduction. A selected sample (x = 0.2) has been studied by neutron powder diffraction (NPD) and X-ray absorption spectroscopy. Both techniques indicate that Fe and Mn adopt a divalent oxidation state, although Fe^{2+} ions are under tensile stress whereas Mn^{2+} ions undergo compressive stress in the structure. The unit-cell parameters progressively evolve from a = 3.9932(4) Å and c = 3.4790(4) Å for x = 0 to a = 4.00861(15) Å and c = 3.46769(16) Å for x = 0.2; the cell volume presents an expansion across the series from V = 55.47(1) to 55.722(4) Å^3 for x = 0 and 0.2, respectively, because of the larger effective ionic radius of Mn^{2+} versus Fe^{2+} in four-fold coordination. Attempts to prepare Mn-rich compositions beyond x = 0.2 were unsuccessful. For $SrFe_{0.8}Mn_{0.2}O_2$, the magnetic properties indicate a strong magnetic coupling between Fe^{2+} and Mn^{2+} magnetic moments, with an antiferromagnetic temperature T_N above room temperature, between 453 and 523 K, according to temperature-dependent NPD data. The NPD data include Bragg reflections of magnetic origin, accounted for with a propagation vector k = ($^1/_2$, $^1/_2$, $^1/_2$). A G-type antiferromagnetic structure was modeled with magnetic moments at the Fe/Mn position. The refined ordered magnetic moment at this position is 1.71(3) μ_B/f.u. at 295 K. This is an extraordinary example where Mn^{2+} and Fe^{2+} ions are stabilized in a square-planar oxygen coordination within an infinite-layer structure. The layered $SrFe_{1-x}Mn_xO_2$ oxides are kinetically stable at room temperature, but in air at ~170 °C, they reoxidize and form the perovskites $SrFe_{1-x}Mn_xO_{3-\delta}$. A cubic phase is obtained upon reoxidation of the layered compound, whereas the starting precursor $SrFeO_{2.875}$ ($Sr_8Fe_8O_{23}$) was a tetragonal superstructure of perovskite.

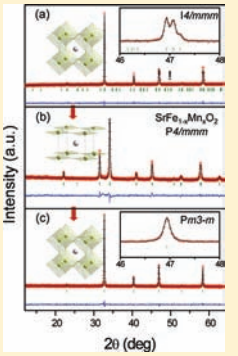

1. INTRODUCTION

Tsujimoto et al.[1] have recently reported a new oxide, $SrFeO_2$, with a novel structure for an oxoferrate, prepared by the topotactical reduction of $SrFeO_{3-d}$ perovskite with CaH_2 under mild temperature conditions. The material presents high-spin Fe^{2+} in a square-planar coordination with "infinite-layer" structure, which is derived from a simple cubic perovskite structure by removal of all of the apical O atoms. As a consequence, the c unit-cell parameter shrinks in a tetragonal structure, isotopic with $SrCuO_2$,[2] with space group $P4/mmm$ (a = 3.9911 Å and c = 3.4748 Å). $SrFeO_2$ contains layers of corner-sharing FeO_4 squares with Sr^{2+} cations in between, similar to the superconducting copper oxides. The Fe−O distances of 1.995 Å are as expected for four-coordinated Fe^{2+}. These cations with d^6 configuration in oxides usually appear in an octahedral or a tetrahedral coordination with O atoms. This square-planar configuration for Fe is very exceptional; it has been previously reported in compounds such as $Sr_3Fe_2O_5$[3] and $Sr_3Fe_2O_4Cl_2$[4] or in Na_4FeO_3[5] and $BaFeSi_4O_{10}$,[6] where the squares are not condensed to each other.

$SrFeO_2$ presents very interesting physical properties. It is magnetically ordered above room temperature ($T_N \cong$ 473 K), which is surprisingly high for a layered, two-dimensional material, on the order of that exhibited by three-dimensional oxides such as NiO ($T_N \cong$ 525 K). In the antiferromagnetically ordered state, the magnetic moments are perpendicular to the c axis. Several theoretical studies have been carried out to understand the mechanisms that govern the magnetism of this material.[7−10] Tsujimoto et al.[1] suggested a $(d_{xz},d_{yz})^3(d_{xy})^1(d_{z^2})^1(d_{x^2-y^2})^1$ electronic configuration for Fe^{2+} in the square-planar coordination. However, this configuration should be subject to orbital ordering or Jahn−Teller distortion when the temperature is lowered, which has not been observed. Moreover, the orientation of the magnetic moments, as revealed by neutron powder diffraction (NPD) analysis, is anomalous. Therefore, previous calculations suggest that the down-spin Fe 3d electrons occupy

Received: July 13, 2011
Published: October 05, 2011

the nondegenerate d_{z^2} level rather than the expected (d_{xz},d_{yz}) states, so the electron configuration would be $(d_{z^2})^2(d_{xz},d_{yz})^2(d_{xy})^1(d_{x^2-y^2})^1$. This state decreases in energy to reduce Coulomb repulsion, accounting for the anomalous crystal and magnetic structures.[8,9]

The same infinite-layer structure has been observed in the solid solution $Sr_{1-x}Ca_xFeO_2$[11,12] and $Sr_{1-x}Ba_xFeO_2$.[13] However, $CaFeO_2$ has a different crystal structure in which there is a distortion of the square plane toward a tetrahedral coordination for Fe^{2+} ions. Also, the defect $Sr_3Fe_2O_5$ Ruddlesden−Popper oxide has been prepared by the same method of synthesis and shows the same high-spin Fe^{2+} ions in a square-planar coordination.[3]

As mentioned before, $SrFeO_2$ was synthesized by reduction of the $SrFeO_{3-\delta}$ perovskite at low temperatures with CaH_2. This is a recently discovered reagent for the kinetically controlled removal of oxygen from oxides. Reduction occurs at very low temperatures, insufficient to rearrange the structure of the starting material, selectively removing some O atoms. However, it has been reported that the synthesis of $SrFeO_2$ is not topotactic.[14] The starting material $SrFeO_{3-\delta}$ contains FeO_6 octahedra; upon heating of this material with CaH_2, some of the O atoms disappear and some of the octahedra transform to intermediate FeO_4 tetrahedra (forming the $SrFeO_{2.5}$ intermediate compound). One of the remaining O atoms moves to a vacant site, forming a FeO_4 square. The Sr and Fe atoms maintain their position in the whole reduction process. Using this procedure, the most thermodynamically stable products are not formed because the temperature is not high enough to produce the required diffusion of the metal atoms; therefore, the final compound is not the most stable one but is the product of the fastest reaction. This reducing agent was first used by Hayward et al.;[15−19] it has been successfully utilized for the synthesis by topotactic reduction of new oxides containing 3d transition elements, e.g., $LaNiO_2$ from $LaNiO_3$ perovskite,[15] $NdNiO_{2+x}$ from $NdNiO_3$,[16] $LaSrCoO_{3.5-x}$ from $LaSrCoO_4$,[17] and $La_{1-x}Sr_xMnO_{2.5}$.[18] This technique was also employed to synthesize a new oxyhydride compound: $LaSrCoO_3H_{0.7}$.[19]

Aiming to increase the options of stabilization of transition-metal ions in a square-planar configuration, we have addressed the preparation of a series of layered oxides of the formula $SrFe_{1-x}Mn_xO_2$ (x = 0.1, 0.2, 0.3) using CaH_2 as the reducing agent at moderate temperatures. We describe the occurrence of Mn^{2+} ions in a square-planar coordination in an infinite-layer structure and describe evolution of the structural and magnetic properties. This is complemented with a X-ray absorption spectroscopy (XAS) study of the oxidation states of Fe and Mn for a selected composition. During the review process of the present manuscript, Seinberg et al.[20] reported some results concerning the same series. There is a basic agreement with the mentioned report; the present paper additionally contributes temperature-dependent NPD data, thermal analysis, magnetic and XAS studies, and investigation of the nature of the reoxidation product.

2. EXPERIMENTAL SECTION

In the synthesis protocol, the first step was the preparation of a series of perovskites $SrFe_{1-x}Mn_xO_{3-\delta}$ by a soft-chemistry procedure. We have dissolved stoichiometric amounts of $Sr(NO_3)_2$, $FeC_2O_4\cdot 2H_2O$, and $MnCO_3$ in citric acid and some drops of nitric acid. The citrate and nitrate solution was slowly evaporated, leading to organic resins that contain a homogeneous distribution of the involved cations. The resins were dried at 120 °C and then decomposed at 600 °C for 12 h. The organic materials and nitrates were eliminated in a subsequent treatment at 800 °C in air for 2 h. This treatment gave rise to finely divided and homogeneous precursor materials. Then, the precursors were ramped at 5 °C min^{-1} up to 1000 °C and annealed at this temperature for 12 h in air to obtain the $SrFe_{1-x}Mn_xO_{3-\delta}$ perovskites. The second step of the synthesis is reduction of the perovskites to give the layered $SrFe_{1-x}Mn_xO_2$ materials. Reduction has been carried out with CaH_2 as the reducing agent. $SrFe_{1-x}Mn_xO_{3-\delta}$ perovskite and 2 M excess of CaH_2 were finely ground in an N_2-filled glovebox, sealed in an evacuated Pyrex tube, and reacted at 583 K for 2 days. The residual CaH_2 and CaO products were removed from the final phase by washing the product with a NH_4Cl/methanol solution.

The characterization was performed by X-ray diffraction (XRD) measurements with a Bruker-AXS D8 diffractometer (40 kV, 30 mA), controlled by *DIFFRACT*^{plus} software, in Bragg−Brentano reflection geometry with Cu Kα radiation (λ = 1.5418 Å). NPD data of the sample with x = 0.2 were collected in the high-resolution powder diffractometer D1A (λ = 1.910 Å) at room temperature and in the D2B instrument (λ = 1.594 Å) at 295, 373, 453, and 523 K at the ILL nuclear reactor in Grenoble, France. Refinement of the crystal and magnetic structures was performed by the Rietveld method,[21] with the *Fullprof* refinement program.[22]

Thermal analysis was carried out in a Mettler TA3000 system equipped with a TC10 processor unit. Thermogravimetric analysis (TGA) curves were obtained in a TG50 unit, working at a heating rate of 10 °C min^{-1}, in air. About 50 mg of the sample was used. Differential scanning calorimetry (DSC) experiments were performed in a DSC30 unit, in the temperature range 35−550 °C. The heating rate was 10 °C min^{-1}, using about 70 mg of the sample.

The magnetic measurements were performed in a commercial SQUID magnetometer from Quantum Design. The direct-current magnetic susceptibility was measured in both zero-field-cooled (ZFC) and field-cooled (FC) conditions in the temperature interval 1.8 K < T < 650 K under a magnetic field of 1 kOe. The isothermal magnetization curves with different hysteresis cycles were obtained at T = 5, 150, and 300 K for applied magnetic fields ranging from −50 to +50 kOe.

XAS measurements have been performed on a $SrFe_{0.8}Mn_{0.2}O_2$ sample. The measurements at the Fe and Mn K-edges were carried out in the fluorescence yield mode at the Spanish CRG beamline (SpLine-BM25A) of the ESRF. The incident beam was monitored by a N_2-filled gas ionization chamber. Fe and Mn Kα fluorescence lines were collected using a 13-element Si(Li) detector (e2v Instruments). Several spectra were taken, in order to improve the signal-to-noise ratio. Several references (Fe, FeO, and α-Fe_2O_3 for iron and Mn, MnO, and Mn_2O_3 for manganese) were used for comparison.

Self-consistent X-ray absorption near-edge structure (XANES) calculations were performed using the real-space multiple scattering formalism of the FEFF8 code.[23] Atomic potentials were approximated by a set of spherical muffin-tin potentials, using the Mattheiss prescription and following the Norman criterion for determination of the atomic radii.[24] An overlapping factor between the atomic potentials of 15% has been imposed. In addition, in order to choose a good approximation for the electronic potential, it has been observed that Coulomb hole correlation effects are crucial for improvement in the reproducibility of the XANES spectrum in the relative positions of its spectral features. Thus, a Hedin−Lundqvist energy-dependent exchange-correlation potential has been selected.[25]

3. RESULTS

3.1. Structural Refinement. As a first step, the $SrFe_{1-x}Mn_xO_{3-\delta}$ precursor perovskites were synthesized and characterized by XRD. The XRD patterns have been indexed in the tetragonal $I4/mmm$ space group similar to the previously reported $Sr_8Fe_8O_{23}$.[26] Subsequently, the $SrFe_{1-x}Mn_xO_2$ (x = 0, 0.1, 0.2)

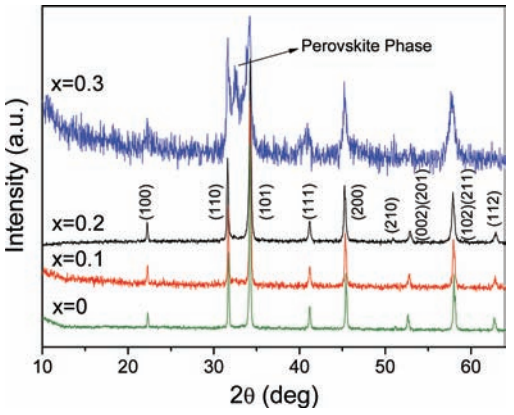

Figure 1. Laboratory XRD patterns for $SrFe_{1-x}Mn_xO_2$ ($x = 0, 0.1, 0.2, 0.3$).

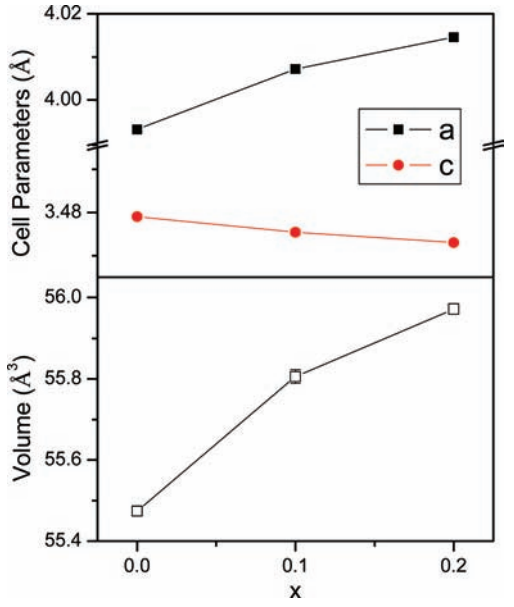

Figure 2. Variation of the unit-cell parameters and volume of $SrFe_{1-x}Mn_xO_2$ for $x = 0$, 0.1, and 0.2.

layered oxides were obtained by controlled reduction of the precursor perovskites. The final products were obtained as black well-crystallized powders. Figure 1 shows the XRD patterns of the $x = 0$, 0.1, 0.2, and 0.3 samples. The compound with $x = 0.3$ and higher values of x could not be synthesized in a crystalline form; the products consisted of a poorly crystallized mixture of the layered and precursor perovskite phases. The XRD patterns of $x = 0$, 0.1, and 0.2 can be indexed in a tetragonal unit cell in the $P4/mmm$ space group with layered structure. Refinement of the crystal structure from XRD data allowed us to determine the unit-cell parameters and volume, represented in Figure 2 as a function of the content of Mn.

In order to gain more information on the structural modification occurring upon Mn introduction, the crystallographic structure of $SrFe_{0.8}Mn_{0.2}O_2$ was refined from the high-resolution NPD pattern collected at room temperature with $\lambda = 1.910$ Å. The $SrFeO_2$ crystal structure was considered as the starting structural model, in the space group $P4/mmm$.[1] We assumed that Sr atoms occupy the 1d ($^1/_2$, $^1/_2$, $^1/_2$) site, Fe and Mn atoms are located at random at the 1a (0, 0, 0) site, and O atoms occupy the

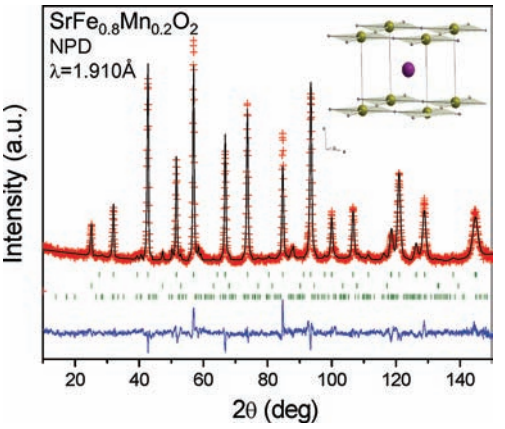

Figure 3. Observed (crosses), calculated (full line), and difference (bottom) NPD Rietveld profiles for $SrFe_{0.8}Mn_{0.2}O_2$ ($\lambda = 1.910$ Å) at 295 K. The second series of tick marks corresponds to the magnetic structure and the third series to minor amounts of the perovskite precursor of composition $Sr_8Fe_8O_{23}$. The upper inset shows the crystal structure of $SrFe_{1-x}Mn_xO_2$, where the central and bigger atom is Sr and the green atoms are Fe/Mn atoms.

2f ($^1/_2$, 0, 0) site. A schematic view of the crystal structure is illustrated in the inset of Figure 3. The occupancy between Fe and Mn was refined, and it is very close to the starting composition. In fact, neutrons are especially suited to distinguish between Fe and Mn given the contrasting scattering lengths for both elements. The refinement of oxygen occupancy gives a full occupancy of the O atoms in the 2f position. The final Rietveld plot after refinement of the structure of $SrFe_{0.8}Mn_{0.2}O_2$ is shown in Figure 3. The second line of the Bragg reflections refers to the magnetic structure because the material is magnetically ordered at room temperature; the magnetic structure will be described afterward. The third line of the Bragg reflection corresponds to an impurity of 7% of the precursor perovskite $SrFe_{1-x}Mn_xO_{3-\delta}$ (space group $I4/mmm$). Table 1 lists the occupancies, the interatomic distances, the oxidation states, and the discrepancy factors after the refinement. The bond valence sum calculation gave valences of Fe +1.93, Mn +2.24, and Sr +1.90. This suggests that the Fe ions are slightly underbonded and the Mn ions are overbonded (which means that O ions are closer to Mn atoms than to Fe atoms), undergoing tensile and compressive stresses, respectively. This is a result of the relatively larger size of Mn^{2+} (0.66 Å) relative to Fe^{2+} (0.64 Å),[27] as will be discussed below.

3.2. Thermal Analysis (DSC and TGA). DSC was used to observe the phase transition due to thermal oxidation of the samples in air. As shown in Figure 4a, there is an exothermic peak associated with the transition from $SrFe_{1-x}Mn_xO_2$ to the perovskite $SrFe_{1-x}Mn_xO_{3-\delta}$. The oxidation temperature obtained by DSC is around 170 °C. This observation indicates the high mobility of O atoms in this compound at very low temperatures, which could be useful for sensor materials, oxygen membranes, or solid oxide fuel cells.

The thermal stability was also studied by TGA in order to determine the oxygen content of the final perovskite. The measurements were also performed in air. Figure 4b illustrates the TGA curve of $SrFe_{0.8}Mn_{0.2}O_2$. The quantity of absorbed oxygen is calculated from the total weight gain, as indicated in the figure, corresponding to 0.53 O atoms; therefore, the final composition of the oxidized perovskite would be $SrFe_{0.8}Mn_{0.2}O_{2.53}$.

Figure 5 compares the XRD patterns of the $SrFe_{0.8}Mn_{0.2}O_{3-\delta}$ perovskite before reduction with CaH_2, subsequently XRD of the

dx.doi.org/10.1021/ic201488w |Inorg. Chem. 2011, 50, 10929–10936

Table 1. Atom Occupancies, Selected Interatomic Distances, Valences,[a] and Discrepancy Factors for $SrFe_{0.8}Mn_{0.2}O_2$ Refined from NPD at 295 K in the *P4/mmm* Space Group [Unit-Cell Parameters a = 4.00861(15) Å, c = 3.46769(16) Å, and V = 55.722(4) Å^3]

atom	occupancy	bond	distance/Å
Sr	1.00	Fe/Mn−O1	2.00430(8)
Fe	0.78(1)	Sr−O1	2.65018(8)
Mn	0.22(1)	O1−O1	2.83452(8)
O1	0.98(1)		

valence[a]		discrepancy factor/%	
Fe	+1.93	R_p	4.40
Mn	+2.24	R_{wp}	5.62
Sr	+1.90	R_{exp}	4.17
		χ^2	1.81
		R_{Bragg}	5.83
		R_{mag}	24.9

[a] The valence is the sum of the individual bond valences (s_i) for Sr−O and (Fe,Mn)−O bonds. Bond valences are calculated as $s_i = \exp[(r_0 - r_i)/B]$; B = 0.37 and r_0 = 2.118 for the $Sr^{2+}-O^{2-}$ pair; for the $Fe^{2+}-O^{2-}$ and $Mn^{2+}-O^{2-}$ pairs, r_0 = 1.734 and 1.790, respectively, from ref 42. Individual Sr−O and (Fe,Mn)−O distances (r_i) are taken from this table.

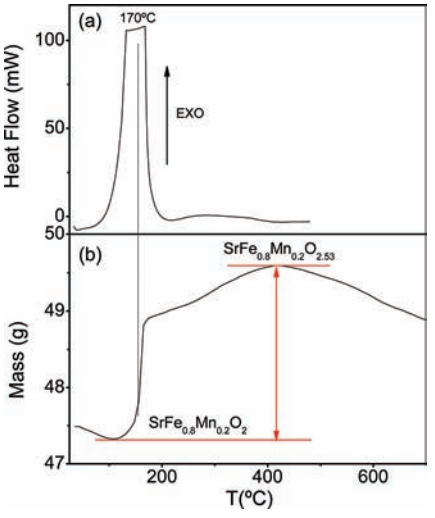

Figure 4. (a) DSC and (b) TGA curves upon reoxidation of $SrFe_{0.8}Mn_{0.2}O_2$ in an air atmosphere.

layered compound, and finally the XRD diagram of the perovskite after oxidation of the layered compound at 1000 °C during 4 h in air. Figure 5 shows that the final perovskite is even more crystalline than the initial one and that it has a higher symmetry; it can be well refined in the cubic $Pm\bar{3}m$ space group, whereas the precursor perovskite is tetragonal (space group $I4/mmm$). The insets of Figure 5 show a characteristic reflection of the tetragonal (Figure 5a) and cubic (Figure 5c) phases. If we compare the unit-cell parameters of the cubic aristotype of the tetragonal phase, a_0 = 3.854(1) Å, and of the final oxidized phase, a = 3.8675(8) Å, the higher value of the parameter in the final perovskite indicates a lower content of oxygen on this reoxidized sample because of the smaller Fe oxidation state of the final perovskite compared to

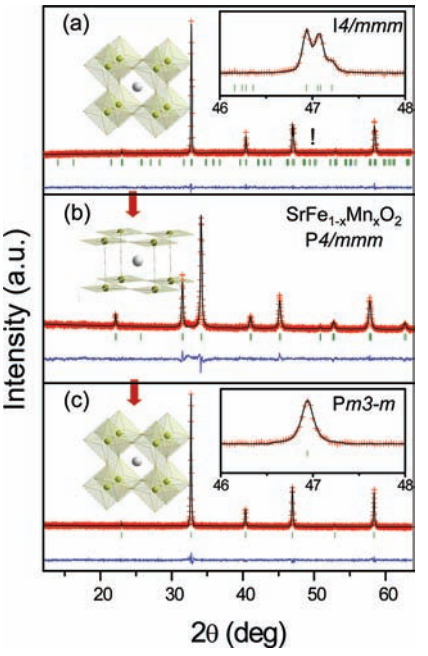

Figure 5. Comparison of the XRD Rietveld profiles of (a) the tetragonal ($I4/mmm$) three-dimensional perovskite precursor of composition $SrFe_{0.8}Mn_{0.2}O_{2.875}$ (the inset shows the splitting of some reflections characteristic of the tetragonal symmetry), (b) the tetragonal infinite-layer structure ($P4/mmm$) of $SrFe_{0.8}Mn_{0.2}O_2$, and (c) the cubic ($Pm\bar{3}m$) $SrFe_{0.8}Mn_{0.2}O_{2.53}$ perovskite obtained by reoxidation of $SrFe_{0.8}Mn_{0.2}O_2$ (the inset shows that the cubic model accounts for the indicated reflection).

the precursor perovskite, which produces an expansion of the cell. It is important to underline that in the $SrFeO_{3-\delta}$ system the only cubic perovskite reported so far is the oxygen-stoichiometric $SrFeO_{3.0}$, which must be prepared under high pressures. The tetragonal $Sr_8Fe_8O_{23}$ perovskite phase stabilized by the solid-state reaction of the citrate precursors shows a long-range ordering of the oxygen vacancies. Reoxidation of $Sr(Fe,Mn)O_2$ can thus be considered as an indirect way to obtain a new cubic $Sr(Fe,Mn)O_{2.5+\delta}$ perovskite phase, where the oxygen vacancies are distributed at random. As we have commented on before, the high mobility of oxide ions predicted for this structural arrangement is potentially useful for applications as sensor materials, oxygen membranes, or in solid oxide fuel cells.

3.3. Magnetic Measurements. The temperature dependence of the susceptibility of $SrFe_{0.8}Mn_{0.2}O_2$, measured under ZFC and FC conditions, is presented in Figure 6a. Both ZFC and FC curves are similar, suggesting the absence of magnetic irreversibilities in this temperature range. The susceptibility presents a broad maximum around 450−500 K that is related to the magnetic ordering temperature and also could be related to the onset of the reoxidation process. The temperature of the maximum is similar to that observed for the parent $SrFeO_2$ compound (T_N = 473 K). A Néel temperature around this temperature has been further confirmed by in situ high-temperature NPD, as described below.

The isothermal magnetization curves measured at 5, 150, and 300 K (Figure 6b) are characteristic of an antiferromagnet with a hysteresis cycle at low fields indicating a canting of the spins, suggesting competitive antiferro- and ferromagnetic interactions, disorder in the lattice, or the effect of some impurity.

3.4. XANES Experiments. The normalized Fe K-edge XANES spectrum of the sample $SrFe_{0.8}Mn_{0.2}O_2$ is shown in Figure 7a.

dx.doi.org/10.1021/ic201488w |*Inorg. Chem.* 2011, 50, 10929–10936

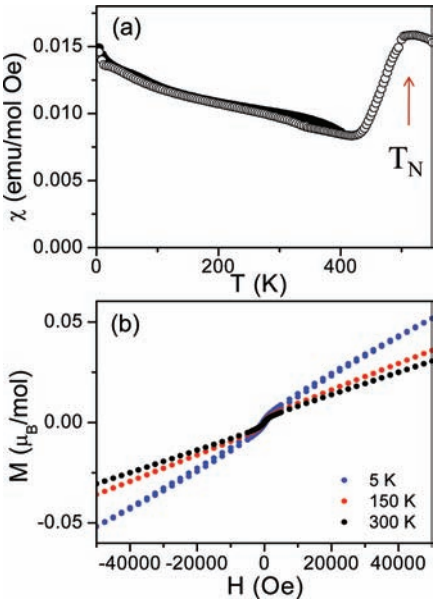

Figure 6. (a) Thermal evolution of the magnetic susceptibility of $SrFe_{0.8}Mn_{0.2}O_2$, recorded with H = 0.1 T, and (b) magnetization isotherms at T = 5, 150, and 300 K.

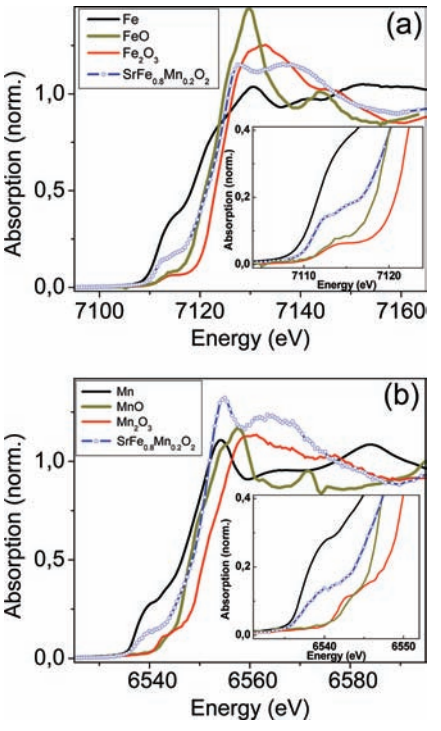

Figure 7. XAS edges for (a) Fe and (b) Mn in $SrFe_{0.8}Mn_{0.2}O_2$.

The spectra of metallic Fe, FeO, and α-Fe_2O_3 were added for comparison. The position of the edge in Figure 7a is consistent with an oxidation state of 2+ for the Fe cations of the specimen. Analogously, the Mn K-edge XANES spectrum of the sample compared with those of the manganese oxide standards, Mn, MnO, and Mn_2O_3, in Figure 7b indicates that the oxidation state of the Mn cations is close to 2+.

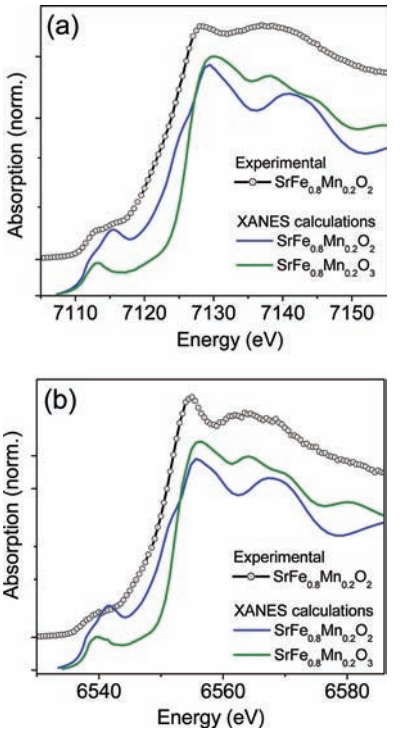

Figure 8. XANES computations at the (a) Fe and (b) Mn K-edges of two possible geometries: square-planar (blue) and octahedral (green) symmetries. The experimental spectra are added for comparison.

Another aspect that should be remarked is that the spectral shapes of both Fe and Mn K-edges are very similar, which suggests that the corresponding geometries of Fe and Mn cations are also similar. In order to confirm the geometry around the Fe and Mn cations, XANES computations have been performed for two different environments. It is well-known that XANES is critically sensitive to the local geometry around an absorbing atom. Here, we have performed calculations for the Fe and Mn K-edges, considering the above-mentioned square-planar geometry, and a typical octahedral geometry, introducing apical O atoms, and considering a $SrFeO_3$ lattice.

First of all, it has been checked that the calculated XANES measurements present a similar spectral shape compared to previous experimental ones.[28,29] The preedge feature and the double structure at 7135 and 7145 eV, in the case of the Fe K-edge, are in good agreement with the experimental XANES. As can be observed in parts a (for Fe) and b (for Mn) of Figure 8, the experimental spectra are better reproduced with a square-planar geometry. The edge positions of the octahedral symmetries appear shifted to higher energies, as expected in cations with higher oxidation state. In contrast, the slope of the edge and the double structure in the preedge feature in the square-planar symmetry matches that of the experimental spectra. However, the main difference between the octahedral and square-planar symmetries has to be located at the beginning of the edge. In the square-planar geometry, apart from the preedge structure, a second peak appears. This low-energy feature is very typical for square-planar geometries and is attributed to electronic transitions from the 1s orbital to the $4p_z$ orbital, lowered by the special two-dimensional symmetry.[30,31] This double feature is supported by our calculations. Therefore, octahedral and square-planar complexes can be distinguished, apart from variation in the edge position due to

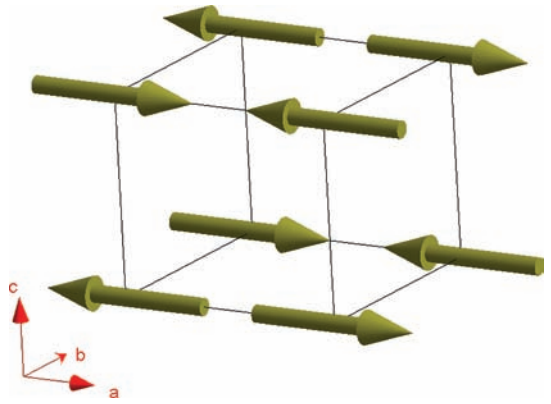

Figure 9. Magnetic structure of $SrFe_{0.8}Mn_{0.2}O_2$ at 295 K, consisting of a G-type antiferromagnetic coupling of (Fe^{2+}, Mn^{2+}) magnetic moments that are lying in the *ab* basal plane of the layered structure.

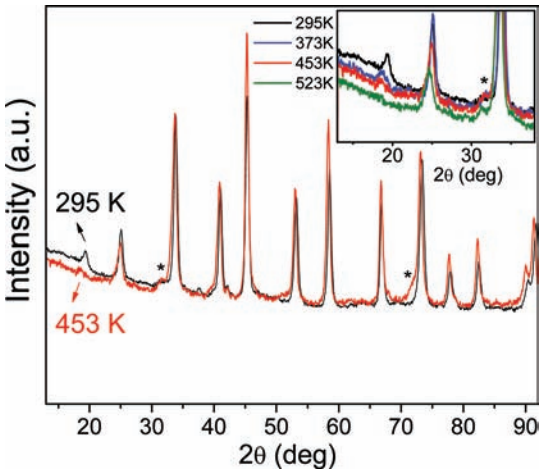

Figure 10. NPD patterns at 295 and 453 K. A small shoulder at $2\theta = 31°$ and 72° (*) indicates the onset of decomposition (reoxidation) of the sample, still magnetic at 453 K. The inset shows thermal evolution of the main magnetic reflection.

modification of the oxidation state, also by the presence or absence of the 1s → $4p_z$ transition.[32] As observed in the experimental spectra (weaker in the Mn edge), the spectra show a double structure, instead of the simple preedge peak obtained in the octahedral coordination (and also checked by previous results). Hence, all of these computations confirm that the square-planar geometry is the major contribution to the experimental spectra.

3.5. Magnetic Structure. The room temperature NPD data of $x = 0.2$ reveal a strong magnetic contribution on the low-angle reflections. Some reflections of magnetic origin appear in the NPD diagram at positions forbidden for the crystallographic Bragg reflections in the tetragonal space group *P*4/*mmm*. The magnetic structure can be defined with a propagation vector $k = (^1/_2, ^1/_2, ^1/_2)$. A G-type antiferromagnetic structure was modeled with magnetic moments at the Fe/Mn position. The refined ordered magnetic moment at this position is 1.71(3) μ_B/f.u. As is schematically illustrated in Figure 9, the magnetic structure is a three-dimensional antiferromagnetic order with magnetic moments perpendicular to the *c* axis; this is the same spin structure as that of the $SrCuO_2$ magnetic insulator. At room temperature, the observed magnetic moment is far from saturation. However, the value previously reported for the magnetic moment in $SrFeO_2$ at room temperature was 3.1 μ_B,[1] significantly higher than our observed value. Certainly, this is a result of the magnetic disordering introduced by the presence of Mn^{2+} cations, randomly distributed with the Fe^{2+} ions over the B positions of the perovskite. The low magnitude of the ordered magnetic moments seems to indicate that the Fe and Mn magnetic moments are not aligned, presenting a canting angle that can be as high as 90° and thus reducing the global magnetic moment observed by neutrons. Because Fe and Mn are totally disordered, we cannot determine the relative orientation of both magnetic moments from a diffraction experiment.

We have performed NPD experiments above room temperature in order to determine the magnetic ordering transition. Figure 10 plots the NPD patterns at 295 and 453 K, evidencing that the main "infinite layer" phase is unchanged, and only a small shoulder at $2\theta = 31°$ and 72° indicates the onset of decomposition (reoxidation) of the sample, still magnetic at 453 K. The inset of Figure 10 shows the fading of the main magnetic peak as the temperature increases. The magnetic peak at 453 K is still present but is very weak, indicating that the magnetic interactions are about disappearing at this temperature. The magnetic peak is completely vanished at 523 K. Therefore, the magnetic transition takes place between these temperatures, confirming the results of the magnetic susceptibility measurements, where a broad peak between 450 and 500 K corresponds to T_N.

4. DISCUSSION

We have successfully synthesized new layered oxides with Fe^{2+} and Mn^{2+} cations in a square-planar configuration with the formula $SrFe_{1-x}Mn_xO_2$ ($x = 0.1, 0.2$). As described for $SrFeO_2$, the powerful reducing reagent CaH_2 is also effective in the topotactical removal of the apical O atoms of the perovskite precursor $SrFe_{1-x}Mn_xO_{3-\delta}$ at very low temperatures. This technique allows stabilization of metastable compounds that are not the most stable thermodynamically, but they are the fastest to be formed at low temperatures. We have determined that the layered phases of the formula $SrFe_{1-x}Mn_xO_2$ are kinetically stable at low temperatures, but in the presence of air at approximately 170 °C, they reoxidize and form the perovskites $SrFe_{1-x}Mn_xO_{3-\delta}$. A cubic phase is obtained upon reoxidation of the layered compound, whereas the starting precursor was an orthorhombic superstructure of perovskite. Also, with time (after some weeks), in the presence of air, $SrFe_{1-x}Mn_xO_2$ slowly decomposes, and this leads to the formation of an oxidized perovskite.

By XRD, we have confirmed the formation of the layered phases and the infeasibility of the synthesis of the crystalline compounds with $x \geq 0.3$. As is shown in Figure 2, the *a* parameter increases and *c* decreases with the Mn content, yielding a global increase of the unit-cell volume with *x*. This is consistent with the larger ionic size of 4-fold-coordinated Mn^{2+} (0.66 Å) versus Fe^{2+} (0.64 Å).[24] Seinberg et al.[20] found a similar evolution of the cell parameters: contraction of *c*, while the *a* parameter increases. This evolution can be explained by taking into account the first-principles calculations performed in $SrFeO_2$, where it seems that the electronic configuration of Fe $3d^6$ electrons is $(d_{z^2})^2(d_{xz},d_{yz})^2(d_{xy})^1(d_{x^2-y^2})^1$. When Fe is replaced by Mn, the occupancy of d_{z^2} would be partially removed because Mn^{2+} is $3d^5$ and its configuration would be $(d_{xz},d_{yz})^2(d_{xy})^1(d_{z^2})^1(d_{x^2-y^2})^1$. Partial depopulation of the d_{z^2} orbitals could explain the contraction of *c* because the repulsions between the out-of-plane orbitals are reduced.

dx.doi.org/10.1021/ic201488w |*Inorg. Chem.* 2011, 50, 10929–10936

A selected compound of nominal composition $SrFe_{0.8}Mn_{0.2}O_2$, studied by NPD, showed an infinite-layer structure containing Fe and Mn atoms randomly distributed over the B sites of the perovskite, with a composition close to the nominal stoichiometry and a full oxygen sublattice. The (Fe,Mn)−O bond lengths, of 2.00430(8) Å, are slightly longer than the Fe−O distances in the parent compound, of 1.9955 Å. By XANES and bond valence sums, we determined that the compound contains Fe^{2+} and Mn^{2+} cations; because both transition metals are distributed at random in the structure, the Fe ions are under tensile stress, whereas the Mn ions are under compressive stress.

The magnetic ordering temperature is well above room temperature (453 K < T_N < 523 K according to NPD data), which is unexpected for two-dimensional materials because usually T_N decays drastically when the dimensionality decreases. This result indicates that, although we are in the presence of a layered compound, the in-plane magnetic interactions are very strong because of the robust hybridization between (Fe, Mn) $d_{x^2-y^2}$ orbitals and O p_{xy} orbitals and the predicted state of the electrons. We are replacing some Fe cations by Mn cations in $SrFeO_2$, thus introducing disorder on the lattice; however, the value of T_N has hardly been modified. Reduction of the *c* parameter when Mn^{2+} is introduced might lead to a stronger interlayer coupling, which would reinforce the magnetic interactions. In addition, compared to the Fe^{2+} ions with the d_{z^2} orbital fully occupied, the Mn^{2+} ions have only one electron in the d_{z^2} orbital, which could also contribute to the magnetic coupling. The magnetic structure is a G-type collinear antiferromagnetic arrangement of (Fe, Mn) spins, with the magnetic moments lying, on average, perpendicular to the *c* axis, as was previously reported for $SrFeO_2$.[1] However, the value of the ordered magnetic moment is noticeably smaller [m = 1.71(3) μ_B/f.u.], which is probably related to the different orientations of Fe^{2+} and Mn^{2+} spins within the basal *ab* plane of the layered structure; this orientation cannot be independently determined in a NPD experiment and, globally, leads to a smaller ordered average moment.

As mentioned before, attempts to prepare Mn-rich compositions beyond x = 0.2 were unsuccessful. Stabilization of $SrMnO_2$ remains a challenge for preparative chemists. However, it is worth mentioning that Mn^{2+} has been seldom stabilized in the square-planar coordination in oxide materials. In the crystal structure of mixed-anion oxypnictides, of composition $A_2Mn_3X_2O_2$ (A = Sr, Ba; X = As, Sb, P), Mn^{2+} is present in CuO_2-type layers, interleaved with more complex layers Mn_2X_2 and A sheets.[33−36] Mn^{2+} cations are in a square-planar coordination in $MnTeMoO_6$.[37] There are also square-planar-coordinated MnO_2 units in the monoclinic $BiMn_7O_{12}$ perovskite[38] and other cubic perovskites of the family $A_3A'Mn_4O_{12}$,[39,40] but in these cases, the square-planar configuration corresponds to Jahn−Teller Mn^{3+} ions. Also, $Rb_{15}Mn_{11}O_{22}$ contains Mn^{2+} in a distorted tetrahedral coordination, and Mn^{3+} approaches a square-planar configuration.[41]

5. CONCLUSIONS

Mn^{2+} ions have been stabilized in an infinite-layer structure in the $SrFe_{1-x}Mn_xO_2$ (x = 0.1, 0.2) series. NPD data and XAS provide evidence that the oxidation state for both ions is divalent. They are both four-fold-coordinated to O atoms in $(Fe,Mn)O_4$ square-planar units that share corners, giving rise to infinite layers separated by Sr^{2+} ions. The magnetic coupling within these layers is extraordinarily strong, as demostrated by a Néel temperature well above room temperature (453 K < T_N < 523 K) and the evidence of antiferromagnetic ordering detected by neutrons at and above room temperature. The reduced observed magnetic moment [1.71(3) μ_B] refined at room temperature may be a consequence of the noncollinear arrangement of Fe^{2+} and Mn^{2+} spins. Reoxidation of $Sr(Fe,Mn)O_2$ at mild temperatures in air leads to a new cubic perovskite phase, distinct from the original precursor perovskite and characterized by a large number of oxygen vacancies distributed at random in the cubic structure.

AUTHOR INFORMATION

Corresponding Author

*E-mail: retuerto@rci.rutgers.edu.

ACKNOWLEDGMENT

We are thankful for financial support of the Spanish Ministry of Science and Technology to Project MAT2010-16404 and to the Spanish Ministry of Education and the Fulbright Commission for a grant to Dr. M. Retuerto. We thank Dr. M. García-Hernández for magnetic measurements, Dr. M. Greenblatt for the critical reading of the manuscript, and the ILL for making all facilities available.

REFERENCES

(1) Tsujimoto, Y.; Tassel, C.; Hayashi, N.; Watanabe, T.; Kageyama, H.; Yoshimura, K.; Takano, M.; Ceretti, M.; Ritter, C.; Paulus, W. *Nature* **2007**, *450*, 1062.

(2) Takano, M.; Takeda, Y.; Okada, H.; Miyamoto, M.; Kusaka, T. *Physica C* **1989**, *159*, 375.

(3) Kageyama, H.; Watanabe, T.; Tsujimoto, Y.; Kitada, A.; Sumida, Y.; Kanamori, K.; Yoshimura, K.; Hayashi, N.; Murakana, S.; Takano, M.; Ceretti, M.; Paulus, W.; Ritter, C.; Andre, G. *Angew. Chem., Int. Ed.* **2008**, *47*, 5740.

(4) Dixon, E.; Hayward, M. A. *Inorg. Chem.* **2010**, *49*, 9649.

(5) Rieck, H.; Hoppe, R. *Z. Anorg. Allg. Chem.* **1977**, *437*, 95.

(6) Hazen, R. M.; Burnham, C. W. *Am. Mineral.* **1974**, *59*, 1166.

(7) Kohler, J. *Angew. Chem., Int. Ed.* **2008**, *47*, 4470.

(8) Xiang, H. J.; Wei, S. H.; Whangbo, M. H. *Phys. Rev. Lett.* **2008**, *100*, 167207.

(9) Pruneda, J. M.; Íñiguez, J.; Canadell, E.; Kageyama, H.; Takano, M. *Phys. Rev. B* **2008**, *78*, 115101.

(10) Ju, S.; Cai, T.-Y. *Appl. Phys. Lett.* **2009**, *94*, 061902.

(11) Tassel, C.; Watanabe, T.; Tsujimoto, Y.; Hayashi, N.; Kitada, A.; Sumida, Y.; Yamamoto, T.; Kageyama, H.; Takano, M.; Yoshimura, K. *J. Am. Chem. Soc.* **2008**, *130*, 3764.

(12) Tassel, C.; Pruneda, J. M.; Hayashi, N.; Watanabe, T.; Kitada, A.; Tsujimoto, Y.; Kageyama, H.; Yoshimura, K.; Takano, M.; Nishi, M.; Ohoyama, K.; Mizumaki, M.; Kawamura, N.; Iñiguez, J.; Canadell, E. *J. Am. Chem. Soc.* **2009**, *131*, 221.

(13) Yamamoto, T.; Li, Z.; Tassel, C.; Hayashi, N.; Takano, M.; Isobe, M.; Ueda, Y.; Ohoyama, K.; Yoshimura, K.; Kobayashi, Y.; Kageyama, H. *Inorg. Chem.* **2010**, *49*, 5957.

(14) Hayward, M. A.; Rosseinsky, M. J. *Nature* **2007**, *450*, 960.

(15) Hayward, M. A.; Green, M. A.; Rosseinsky, M. J.; Sloan, J. *J. Am. Chem. Soc.* **1999**, *121*, 8843.

(16) Hayward, M. A.; Rosseinsky, M. J. *Solid State Sci.* **2003**, *5*, 839.

(17) Hayward, M. A.; Rosseinsky, M. J. *Chem. Mater.* **2000**, *12*, 2182.

(18) Casey, P. S.; Barker, D.; Hayward, M. A. *J. Solid State Chem.* **2006**, *179*, 1375.

(19) Hayward, M. A.; Cussen, E. J.; Claridge, J. B.; Bieringer, M.; Rosseinsky, M. J.; Kiely, C. J.; Blundell, S. J.; Marshall, I. M.; Pratt, F. L. *Science* **2002**, *295*, 1882.

(20) Seinberg, L.; Yamamoto, T.; Tassel, C.; Kobayashi, Y.; Hayashi, N.; Kitada, A.; Sumida, Y.; Watanabe, T.; Nishi, M.; Ohoyama, K.;

Yoshimura, K.; Takano, M.; Paulus, W.; Kageyama, H. *Inorg. Chem.* **2011**, *50* (9), 3988.
(21) Rietveld, H. M. *J. Appl. Crystallogr.* **1969**, *2*, 65.
(22) Rodriguez-Carvajal, J. *Physica B* **1993**, *55*, 192.
(23) Ankudinov, A. L.; Ravel, B.; Rehr, J. J.; Conradson, S. D. *Phys. Rev. B* **1998**, *58*, 5765.
(24) Mattheiss, L. *Phys. Rev. A* **1964**, *133*, 1399.
(25) Hedin, L.; Lundqvist, B. I. *J. Phys. C* **1971**, *4*, 2064.
(26) Hodges, J. P.; Short, S.; Jorgensen, J. D.; Xiong, X.; Dabrowski, B.; Mini, S. M.; Kimball, C. W. *J. Am. Chem. Soc.* **2000**, *151*, 190.
(27) Shannon, R. D. *Acta Crystallogr., Sect. A* **1976**, *32*, 751.
(28) Tuilier, M. H.; Buffat, B. *J. Phys. Colloque* **1986**, *C8*, 771.
(29) Okube, M.; Furukawa, Y.; Yoshiasa, A.; Hashimoto, T.; Sugahara, M.; Nakatsuka, A. *J. Phys.: Conf. Ser.* **2008**, *121*, 092004.
(30) Smith, T. A.; Penner-Hahn, J. E.; Berding, M. A.; Doniach, S.; Hodgson, K. O. *J. Am. Chem. Soc.* **1985**, *107*, 5945.
(31) Chen, L. X.; Jäger, W. J. H.; Jennings, G.; Gosztola, D. J.; Munkholm, A.; Hessler, J. P. *Science* **2001**, *292*, 262.
(32) Feth, M. P.; Klein, A.; Bertagnolli, H. *Eur. J. Inorg. Chem.* **2003**, 839.
(33) Brechtel, E.; Cordier, G.; Schafer, H. *Z. Naturforsch. B* **1979**, *34*, 777.
(34) Stetson, N. T.; Kauzlarich, S. M. *Inorg. Chem.* **1991**, *30*, 3969.
(35) Brock, S. L.; Hope, H.; Kauzlarich, S. M. *Inorg. Chem.* **1994**, *33*, 405.
(36) Brock, S. L.; Kauzlarich, S. M. *J. Alloys Compd.* **1996**, *241*, 82.
(37) Doi, Y.; Suzuki, R.; Hinatsu, Y.; Ohoyama, K. *J. Phys.: Condens. Matter* **2009**, *21*, 046006.
(38) Okamoto, H.; Imamura, N.; Karppinen, M.; Yamauchi, H.; Fjellvag, H. *Inorg. Chem.* **2010**, *49*, 8709.
(39) Muñoz, A.; Martínez-Lope, M. J.; Retuerto, M.; Falcón, H.; Alonso, J. A. *J. Appl. Phys.* **2008**, *104*, 083911.
(40) Retuerto, M.; Martínez-Lope, M. J.; Sánchez-Benítez, J.; García-Hernández, M.; Fernández-Díaz, M. T.; Alonso, J. A. *J. Appl. Phys.* **2010**, *108*, 083905.
(41) Nuss, J.; Pfeiffer, S.; van Smaalen, S.; Jansen, M. *Acta Crystallogr.* **2010**, *B66*, 27.
(42) Brese, N. E.; O'Keeffe, M. *Acta Crystallogr., Sect. B* **1991**, *47*, 192.